applied sciences

MDPI

Article

Nozzle Design of Plug-and-Play Passive Pre-Chamber Ignition Systems for Natural Gas Engines

Wei Li [1,2], Junfang Ma [1], Tao Zhu [1,2], Haiqiao Wei [1,*] and Jiaying Pan [1,*]

[1] Weichai Power Co., Ltd., Weifang 261016, China; liwei09@weichai.com (W.L.); majunfang@weichai.com (J.M.); zhutao@weichai.com (T.Z.)
[2] State Key Laboratory of Engines, Tianjin University, Tianjin 300072, China
[*] Correspondence: whq@tju.edu.cn (H.W.); jypan@tju.edu.cn (J.P.)

Abstract: To evaluate the significance of the geometrical parameters of a passive pre-chamber on engine performance, this study investigated the design of a plug-and-play passive pre-chamber in a 15 L heavy-duty natural gas engine. Multi-dimensional numerical investigations were conducted for parametric studies involving lateral angle, orifice diameter, and vertical angle. A compressive flow solver was employed for Navier–Stoke equations, coupled with detailed sub-models and a chemical kinetic scheme. The combustion model was calibrated and could well predict the engine combustion and operating performance. Seven pre-chamber schemes were evaluated, and four optimal ones were selected for experimental tests. The characteristics of the scavenging process, turbulent jet ignition, and main-chamber combustion were investigated and analyzed. The results show that, considering the trade-off between the ignition energy and the scavenging efficiency, the ratio of the pre-chamber to clearance volume is recommended to be 0.2~0.7%, and the corresponding area–volume ratio is 0.003~0.006 mm^{-1}. Compared with the original natural gas engine, the pre-chamber retrofit can save up to 13.2% of fuel consumption, which presents a significant improvement in fuel economy.

Keywords: natural gas engine; turbulent jet ignition; pre-chamber; scavenging; fuel consumption

Citation: Li, W.; Ma, J.; Zhu, T.; Wei, H.; Pan, J. Nozzle Design of Plug-and-Play Passive Pre-Chamber Ignition Systems for Natural Gas Engines. *Appl. Sci.* **2023**, *13*, 9468. https://doi.org/10.3390/app13169468

Academic Editor: Satoru Okamoto

Received: 20 May 2023
Revised: 14 August 2023
Accepted: 17 August 2023
Published: 21 August 2023

1. Introduction

Driven by increasingly stringent fuel consumption and emission regulations [1], the powertrain industry has striven for innovation to meet the ambitious greenhouse gas and CO_2 reduction targets [2,3]. For long-haul transportation, heavy-duty engines are still expected to dominate the market in the foreseeable future. Further efforts, however, still need to be focused on the improvement of thermal efficiency and pollution emissions. Natural gas is an attractive alternative fuel, due to its low carbon emissions and less expensive after-treatment device [4]. An inherent advantage over other fossil fuels is that natural gas can be renewable, and even has a potentially negative carbon impact [5]. The disadvantage lies in its lower efficiency, which is due to knocking limits and low combustion speed.

In recent years, different technologies for improving thermal efficiency have been proposed, such as cooled exhaust gas recirculation (EGR), direct injection, high-energy ignition, lean-burning, miller cycle combined with high compression ratio, pre-chamber (PC), etc. [6–8]. The lean-burning technology is considered a promising solution, thanks to its higher specific heat ratio and lower auto-ignition tendencies. However, its application is limited due to the requirement of specific three-way catalysts in its after-treatment systems. The PC ignition concept (or turbulent jet ignition) can shift the flammability limits towards a higher dilution tolerance, due to enhanced turbulence and increased flame propagation [9,10], which leads to considerably improved ignition and combustion performance under lean-burning conditions.

Depending on whether there is a supply of auxiliary fuel or not, jet ignition is classified into two forms, i.e., active and passive schemes [11–14]. To investigate the ignition and flame dynamics, various experimental [15–17] and numerical studies [18,19] have been carried out. Different single-fuel [20–23] and dual-fuel concepts [24] have been validated, and a new reactivity stratification with a hydrogen turbulent jet to enhance ammonia combustion has also been proposed recently [25,26]. Liu [27] assessed the effects of the PC on combustion characteristics under lean-burning conditions and found that a larger PC volume allowed faster pressure buildup but led to higher heat transfer losses. Antolini [28] evaluated the effect of orifice diameter on the jet characteristics and main chamber (MC) combustion in an optically accessible single-cylinder SI engine. High-speed broadband chemiluminescence imaging was used to track the jet penetration and flame front propagation. Despite the highest flame development angle, the PC with a 1.0 mm orifice diameter presented the lowest combustion duration. Zhu [29] investigated three passively fueled spark plugs with a stoichiometric mixture and different geometries, including orifice diameter, volume, area, and area-to-volume (A/V) ratio. They found that asymmetric orifice sizes yielded slightly more significant variability and delayed flame development. Frasci [30] numerically investigated the effects of passive PC geometry, and their results demonstrated that the highest engine efficiency was achieved at a medium-to-high PC volume and large diameter, both in stoichiometric and lean-burn conditions. Rajasegar [31] explored the EGR dilution limits of a PC-ignited engine operated at stoichiometric conditions and found that the presence of residuals within the PC led to slower spark kernel development. Despite these studies, the effects of the main geometrical parameters of a passive PC on the scavenge and subsequent combustion processes are still not fully understood, especially for heavy-duty gas engine fueling with stoichiometric mixtures and EGR.

In this sense, the current study aims to evaluate the effects of the main geometrical parameters, including the orifice diameter, vertical angle, and lateral angle, on the scavenge, turbulent jet, and combustion characteristics of a novel passive PC in an in-line six-cylinder 14.6 L gas engine. Numerical simulations based on CONVERGE were used to track the residual CO_2 mass fraction and turbulent kinetic energy (TKE) distribution inside the PC, jet penetration, and flame front propagation of seven design cases. Keeping the same knocking frequency and cyclic variations, the in-cylinder pressure, EGR rate, and fuel consumption results were compared in bench tests under four operating conditions. The current work provides useful insights into the PC design and combustion control of heavy-duty gas engines with turbulent jet ignition.

2. Methodology and Specification

2.1. Test Cases

The nozzles connecting the PC and MC affect the scavenging and ejection processes significantly. The critical parameters of the nozzle include orifice diameter, number, and lateral/vertical angle. The orifice diameter and number together affect the ratio of the total orifice cross-sectional area to the PC volume, i.e., the area–volume ratio. Previous studies have shown that the scavenging and flow characteristics of PCs with the same area–volume ratio are similar. An obvious inference of this is that, no matter whether the parameter to be changed is the orifice diameter or the orifice number, the goal is to search for the optimal area–volume ratio. Therefore, the orifice number constant remains while the effects of the orifice diameter and other vital parameters are investigated.

Figure 1 is a structural diagram of the PC. The PC has a cylinder with an inner diameter of 9.6 mm and a volume of 1500 mm^3, which is threaded to fit a standard spark plug. To facilitate rapid replacement without modifying the cylinder head, the plug-and-play PC is designed to match the cavity originally intended for spark plugs, which enables seamless integration between the PC and the combustion chamber. The nozzle adopts a five-orifice design, including four circumferential orifices and one central orifice. The nozzle design parameters include orifice diameter d, vertical angle α, and lateral angle β. The test cases are shown in Table 1. Based on Case 1, with the best economy, the other six cases are also designed to study the effects of d, α, and β on scavenging, ejection, and combustion performance. The vertical angle is within the range of 120~140° to ensure the entrance of the jet flame into the MC at an appropriate angle. The lateral angle is between 0 and 20° to ensure acceptable scavenging. The orifice diameter is between 1.0 and 1.6 mm, which is recommended by the ratio of the total orifice area to pre-chamber volume.

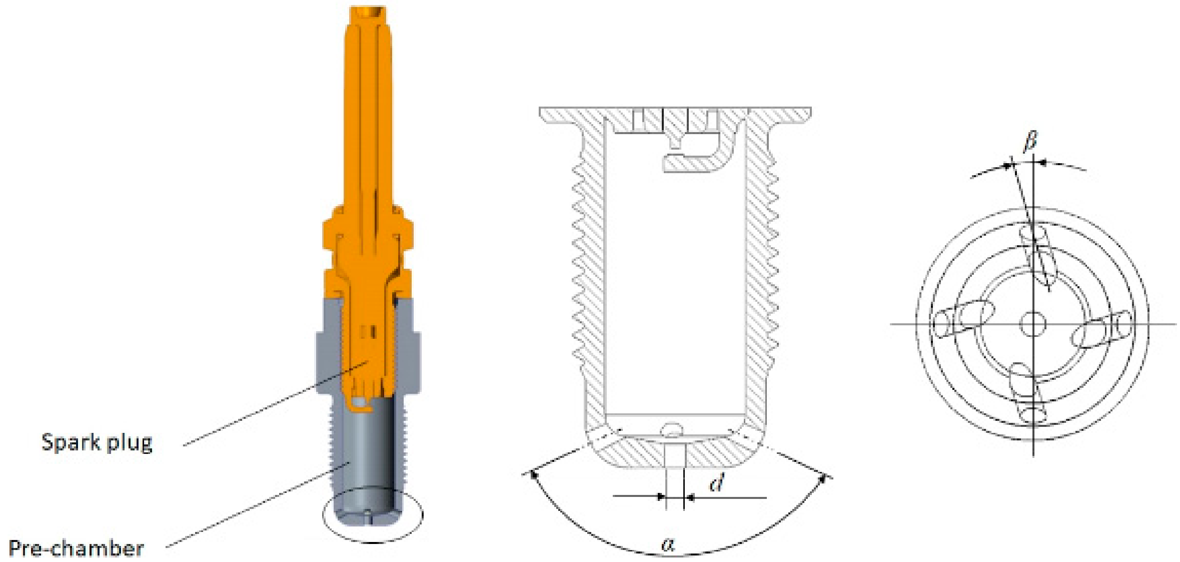

Figure 1. Design parameters of the passive PC nozzle, including orifice diameter d, vertical angle α, and lateral angle β.

Table 1. The test cases for passive PC nozzle research.

Case	d (mm)	α (°)	β (°)
1	1.3	130	10
2	1.3	130	0
3	1.3	130	20
4	1.3	120	10
5	1.3	140	10
6	1.0	130	10
7	1.6	130	10

2.2. Experimental Setup (Figure 2)

The bench test was carried out on the natural gas engine WP15NG, mass-produced by Weichai Power Co., Ltd. The test engine specifications are shown in Table 2. The in-line 6-cylinder engine adopts a turbocharger, intercooler, and EGR, maintaining stoichiometric combustion through an electronic control unit. A direct current dynamometer is used to control the engine speed and torque. The natural gas consumption, intake flow, and air–fuel ratio are closed-loop controlled by INCA software. Six Kistler piezoelectric sensors measure the pressure signals in the respective cylinder with a crank angle resolution of 0.1°CA. More information on the test bench can be found in the literature. Benefiting from the plug-and-play design of the passive PC, the quick retrofit of different schemes improves the efficiency of the test evaluation. To mimic realistic natural gas combustion, there is 14.6% EGR maintained in the natural gas–air mixtures before combustion. A fresh fuel–air mixture contains 72.3% N_2, 22.2% O_2, and 5.5% CH_4, while the EGR contains 72.2% N_2, 0.3% O_2, 15.3% CO_2, and 12.2% H_2O in mass fraction.

Table 2. Test engine specifications.

Item	Value
Engine type	In-line six-cylinder, four-stroke
Intake system	Turbocharged, intercooler, cooled EGR
Bore	136 mm
Stroke	167 mm
Displacement	14.6 L
Compression ratio	12.5
Rated power/speed	390 kW/1700 rpm
Maximum torque/speed	2500 N·m/950~1350 rpm

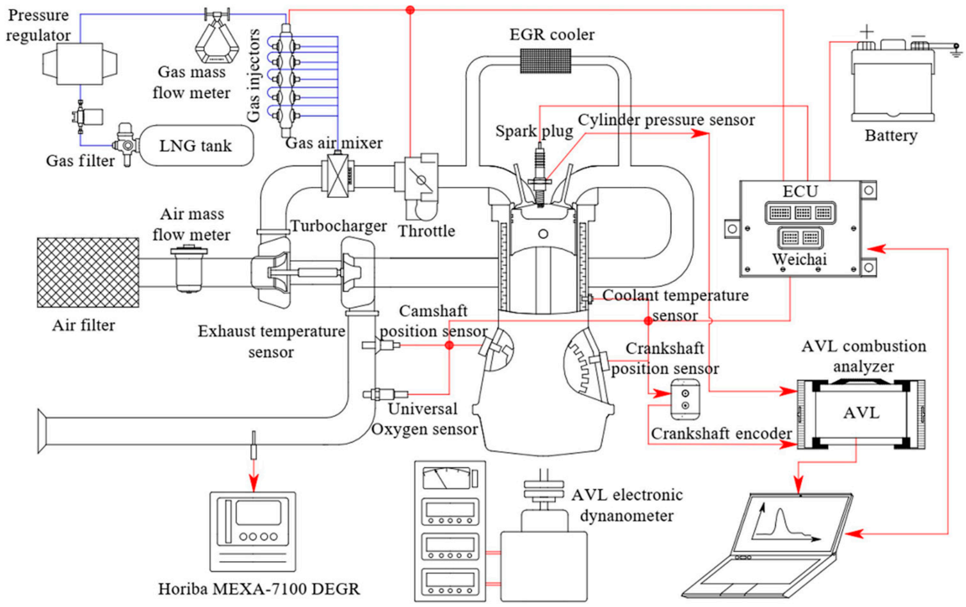

Figure 2. Schematic of the experimental setup.

The operating conditions of the six-cylinder commercial vehicle engine were selected according to the Worldwide Harmonized Heavy-Duty Vehicles Test Procedure, as shown in Table 3, with 1100 rpm and 2000 N·m representing the typical operating conditions. The sensitivity of different PC configurations to operating conditions can be evaluated by varying the engine speed and load. Cylinder pressure signals were recorded with 0.1° crank angle resolution and averaged over 50 consecutive engine cycles. The combustion duration was defined as the crank angle difference between 10% and 90% of the mass fraction burned.

Table 3. Bench test operating conditions.

Cases	Speed (rpm)	Torque (N·m)	Conditions	Power (kW)	BMEP (MPa)	BTE (%)
1	900	1000	Low speed, low load	94	0.87	36.0
2	1100	2000	Normal power	230	1.73	40.3
3	1100	2500	Low speed, high load	288	2.16	40.3
4	1700	2190	Rated power	390	1.90	39.3

2.3. Numerical Model and Calibration

Based on the boundary conditions provided by the one-dimensional simulation software GT-POWER, this study used the three-dimensional computational fluid dynamics software CONVERGE to describe the flow, heat transfer, and combustion phenomena. The spatial discretization of the transport equations adopted the second-order upwind numerical scheme. The time integration took the implicit format, with the time step determined by the Courant–Friedrichs–Lewy condition. The PISO algorithm was used for the pressure–velocity coupling. On the other hand, the RNG k-ε model was used for turbulence simulation because it is effective and can reproduce statistically averaged flow patterns of the LES model (Table 4). The ignition process adopted the source/sink model, releasing 40 mJ of ignition energy in each cycle. Figure 3 shows the computational domain, of which the hybrid meshing process used adaptive refinement to capture the temperature and velocity gradients. The grid independence verification shows that, when the elemental size was below 4 mm, the cylinder pressure became consistent. The G-Equation modeled the flame dynamics, and the laminar flame velocity was corrected to match the experimental cylinder pressure and heat release rate curves.

Table 4. Sub-models for physical and chemical phenomena.

Physical Phenomenon	Sub-Model
Turbulence	RNG k-ε model
Boundary layer	Enhanced wall treatment
Multiphase flow	Species transport model
Ignition	Source/sink model
CH_4 combustion	Opt. GRI-Mech 3.0
NO_x emission	Extended Zeldovich mechanism

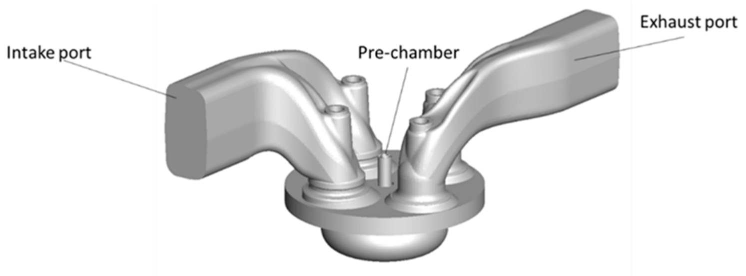

(**a**) Engine CFD geometry

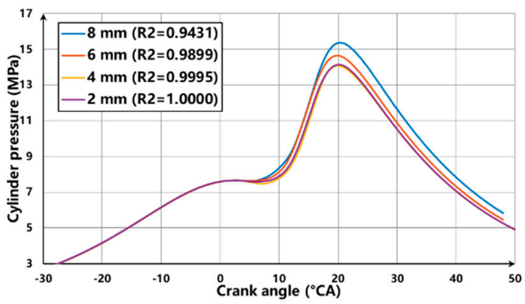

(**b**) Grid independence verification

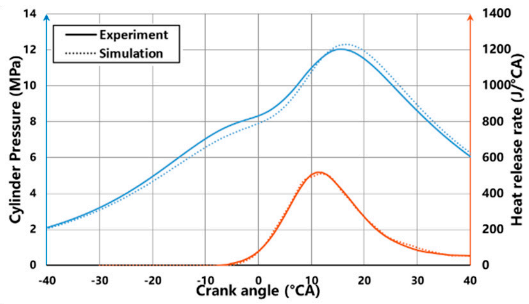

(**c**) Experimental calibration

Figure 3. Computational domain, grid independence verification, and experimental calibration.

The governing equations of mass, species, momentum, and energy transport are given as follows:

$$\frac{\partial \rho}{\partial t} + \nabla \cdot (\rho \boldsymbol{v}) = 0 \tag{1}$$

$$\frac{\partial}{\partial t}(\rho Y_i) + \nabla \cdot (\rho \boldsymbol{v} Y_i) = \nabla \cdot (\rho D \nabla Y_i) + \dot{\rho}_i \tag{2}$$

$$\frac{\partial}{\partial t}(\rho \boldsymbol{v}) + \nabla \cdot (\rho \boldsymbol{v}\boldsymbol{v}) = -\nabla p + \nabla \cdot \boldsymbol{\tau} - \frac{2}{3}\nabla(\rho k) \tag{3}$$

$$\frac{\partial}{\partial t}(\rho e) + \nabla \cdot (\rho \boldsymbol{v} e) = -\nabla \cdot \dot{\boldsymbol{q}}_s - p \nabla \cdot \boldsymbol{v} + \rho \varepsilon + \dot{q_V} \tag{4}$$

where ρ, $\boldsymbol{v}$, e, and Y_i represent density, velocity, internal energy, and mass fraction of species i, respectivley. p, $\boldsymbol{\tau}$, k, and ε represent pressure, stress tensor, turbulence kinetic energy, and turbulence energy dissipation, respectively. $\dot{\boldsymbol{q}}_{\boldsymbol{s}}$ and $\dot{q_V}$ represent the surface heat flux and volume heat source, respectivley. $\dot{\rho}_i$ and D represent the chemical mass source term and mass diffusion coefficient, respectivley.

The reduced natural gas mechanism from GRI 3.0 is formulated as follows:

$$\sum_{i=1}^{N_s} \nu_{ij}^f C_i \leftrightharpoons \sum_{i=1}^{N_s} \nu_{ij}^b C_i,\ j = 1, 2, \ldots, N_r \tag{5}$$

where ν_{ij}^f and ν_{ij}^b represent the matrix of the stoichiometric coefficients for the forward and backward reactions, respectivley. C_i represents the molar concentration of species i. N_r and N_s represent the number of reactions and species, respectivley.

Hence, the chemical source terms can be given by:

$$\dot{\rho}_i = M_i \sum_{j=1}^{N_r} \left(\nu_{ij}^b - \nu_{ij}^f\right) \dot{\omega}_j \tag{6}$$

$$\dot{q_V} = M_i \sum_{j=1}^{N_r} q_j \dot{\omega}_j \tag{7}$$

where M_i represents the molecular weight of species i, and

$$\dot{\omega}_j = k_j^f \prod_{i=1}^{N_s} C_i^{\nu_{ij}^f} - k_j^b \prod_{i=1}^{N_s} C_i^{\nu_{ij}^b} \tag{8}$$

$$q_j = \sum_{i=1}^{N_s} \left(\nu_{ij}^f - \nu_{ij}^b\right) (h_i)_f^{ref} \tag{9}$$

where k_j^f and k_j^b represent the constant rate of forward and backward reaction j, respectivley. $(h_i)_f^{ref}$ represents the enthalpy change in species i formation at the reference temperature.

3. Results and Discussion

3.1. Influence of Nozzle Design on Scavenging

Scavenging refers to the removal and remixing process of residual gas in the PC; however, its effect on heat transfer is equally noteworthy. Ideal scavenging can provide a fresh homogeneous mixture to the spark plug and increase the turbulence intensity to accelerate flame propagation. The pressure difference between the PC and the MC drives scavenging. During the intake stroke, part of the residual gas is removed, and less than 15% of the fresh gas is filled. The subsequent filling is completed in the compression stroke, and the compression ratio and operating conditions determine the final residual gas fraction. This study selects low-speed and high-torque operating conditions, where the residual gas fraction reaches the maximum, for scavenging research.

For research convenience, the top dead center of the compression stroke is chosen as the reference point 0°CA. Figure 4 shows a velocity distribution diagram of each PC after ignition, i.e., −9°CA. During the compression stroke, the mixture in the MC is pressed into the PC to form a scavenging flow field. The lateral angle of the nozzle determines the swirl intensity in the PC. In Figure 4b, the lateral angle is 0°, and the different airflows impact each other in the PC. A large amount of kinetic energy is dissipated near the nozzle, which affects the scavenging near the spark plug. When increasing the lateral angle to 20° in Figure 4c, a stable swirl is formed in the PC. However, in this case, the spark plug is just in the low-speed area of the swirl center, which reduces the scavenging efficiency. The 10°

lateral angle in Figure 4a produces an unstable swirl with a gyro-like precession feature, enhancing the scavenging near the spark plugs.

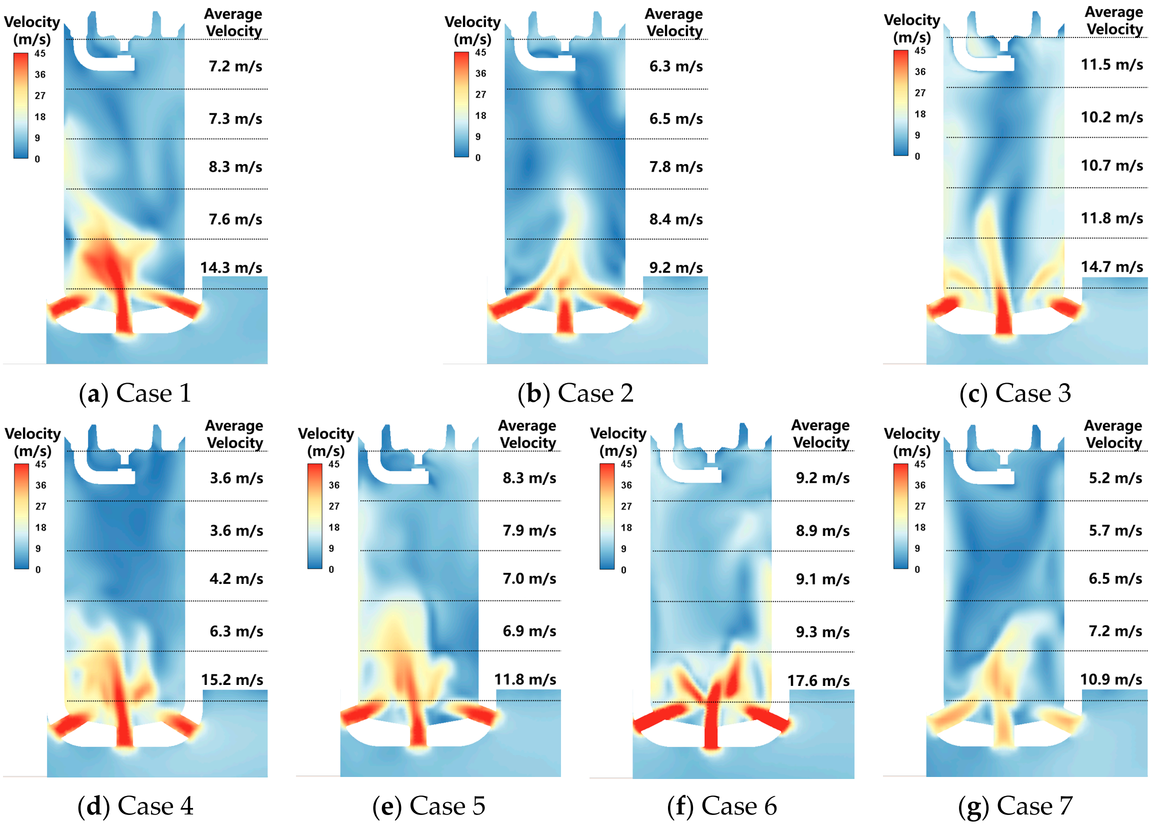

Figure 4. Velocity contours in the pre-camber of 7 cases at −9°CA during scavenging.

On the other hand, the vertical angle of the nozzle is another factor that affects the swirl intensity. In Figure 4d, the vertical angle is 120°, decreasing the swirl radius. Much kinetic energy is dissipated near the nozzle, similar to that of Figure 4b, which is unfavorable for ignition. When the vertical angle increases to 140°, as shown in Figure 4e, the swirl intensity increases but the swirl height decreases, resulting in a decline in the airflow near the spark plug. The influence of the orifice diameter is more intuitive than the nozzle angles. Figure 4f, with a diameter of 1.0 mm, has the highest swirl strength among all of the schemes. Although the flow in Figure 4g, with a diameter of 1.6 mm, is the smoothest, the exhaust gas residue is the lowest, thanks to the highest area–volume ratio. Of course, this is at the cost of reducing the jet penetration distance.

To further study the influence of the nozzle design on the residual gas fraction, Figure 5 shows the mass fraction of carbon dioxide in each PC at −9°CA. It can be seen that the carbon dioxide distribution near the nozzle is highly correlated with the velocity distribution. Near the spark plug, however, there is always a considerable amount of carbon dioxide remaining, regardless of the local velocity. Therefore, the residual carbon dioxide concentration at the spark plug and the distribution uniformity in the PC are critical indicators for evaluating the scavenging efficiency. The former can determine the ignition energy, and the latter can determine the stability of flame propagation. Among all of these schemes, Figure 5g has the lowest residual gas and the most uniform distribution, with an orifice diameter of 1.6 mm. However, due to the increase in the area–volume ratio, the subsequent jet penetration distance decreases, which is unfavorable for the ignition of the MC. In this study, the recommended area–volume ratio was 0.003~0.006 mm^{-1}. The lateral angles in Figure 5a,b are 10° and 0°, respectively. Their residual gas is comparable, but the unstable swirl flow in Figure 5a makes the residual gas distribution more uniform and increases the ignition stability. Figure 5c, Figure 5d, and Figure 5e have a large amount of residual gas remaining in the top area of the PC, but for different reasons. Figure 5c has a lateral angle of 20° and a vertical angle of 130°. Its steady swirl spontaneously concentrates the residual gases towards the center. The lateral angle in Figure 5d is 10° and the vertical angle is 120°. The linear velocity and radius of the swirling flow decrease synchronously, and the stable swirl still gathers the residual gas towards the center. Figure 5e has lateral and vertical angles of 10° and 140°, respectivley. The height and stability of the swirl flow are reduced, therefore, the residual gas is squeezed toward the top and one side area of the PC.

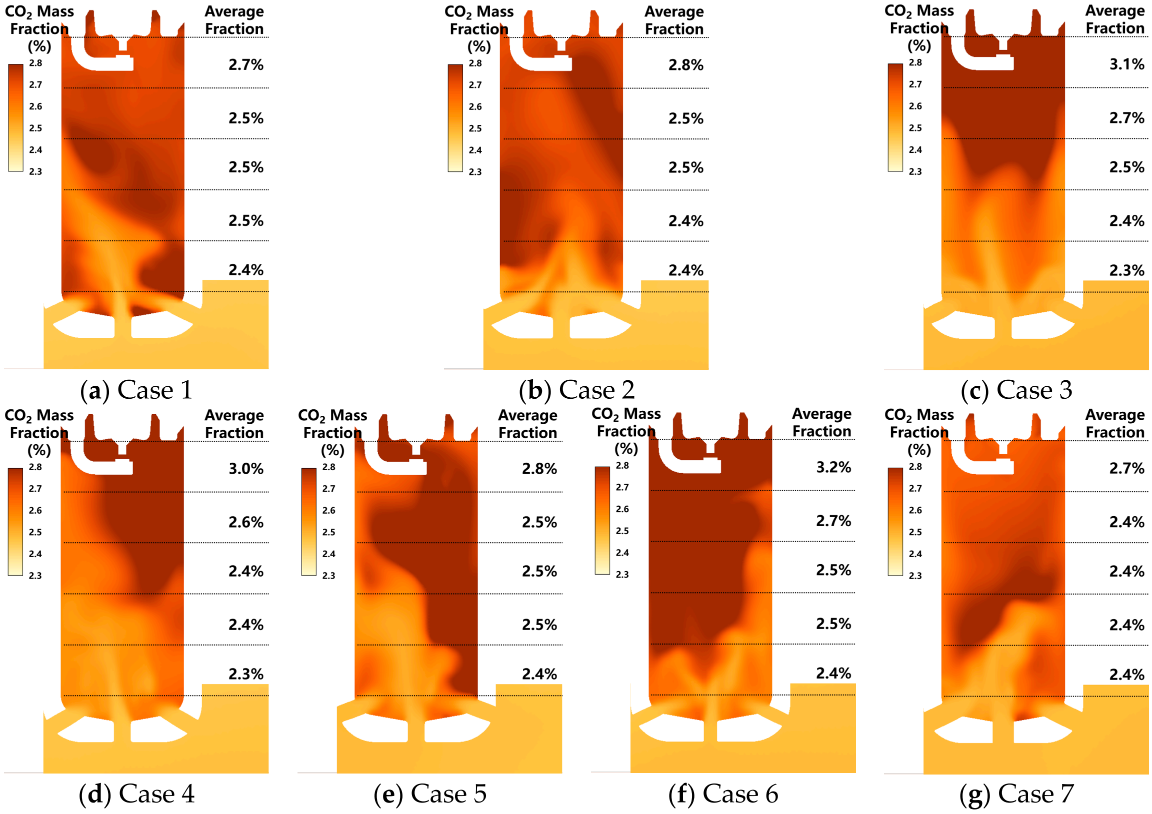

Figure 5. Residual CO_2 mass fraction in the PC of 7 cases at −9°CA during scavenging.

High turbulent kinetic energy can support faster flame propagation and improve efficiency. Figure 6 shows the distribution of turbulent kinetic energy for each PC at −9 °C. As the lateral angle increases, the turbulent kinetic energy level decreases rapidly. In Figure 6c, with a maximum lateral angle of 20°, the turbulent kinetic energy near the spark plug tends to be zero, which is not conducive to the propagation of initial fire nuclei. In Figure 6b, the turbulent kinetic energy level reaches the highest value, with a lateral angle of 0°; however, the high CO_2 concentration near the spark plug offsets this advantage. The trade-off between the turbulent kinetic energy and the CO_2 concentration is also reflected in the influence of the orifice diameter. In Figure 6f, the average turbulent kinetic energy near the orifice region reaches the highest value, compared to the other schemes. However, the CO_2 near the spark plug also reaches its maximum, leading to a decreased ignition performance. The influence of the vertical angle is complex. In Figure 6d, with a vertical angle of 120°, the swirl intensity increases, and a turbulent kinetic energy distribution similar to that in Figure 6c appears. The difference between the two swirl flows is worth noting. The swirl flow in Figure 6c is formed near the orifice with more stability. In contrast, the swirl flow in Figure 6d is formed at a higher height with less stability, homogenizing the turbulent kinetic energy distribution.

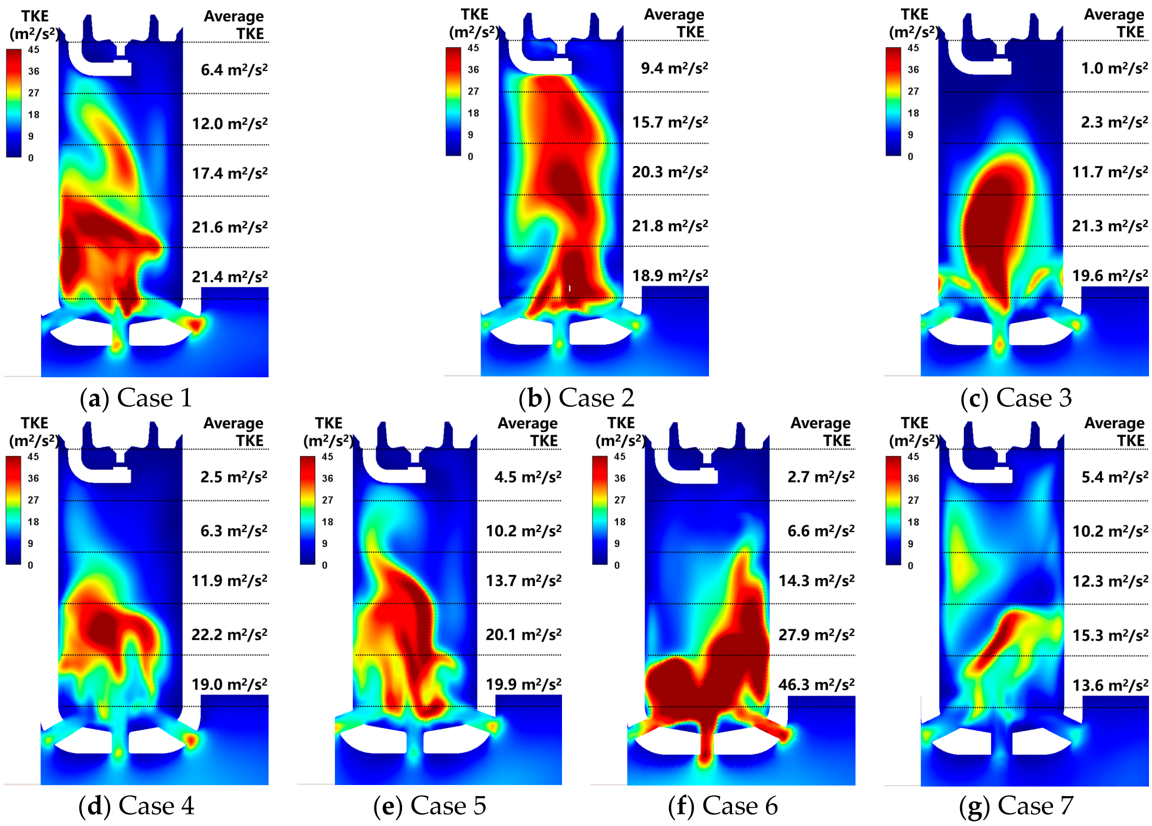

Figure 6. TKE in the PC of 7 cases at −9°CA during scavenging.

In conclusion, the nozzle design should consider the trade-offs of the main parameters. The lateral angle determines the swirl intensity of scavenging. If a stable swirl is formed in the PC, the lateral angle should be appropriately reduced. If the swirl intensity is so slight that the airflows impact each other, the lateral angle should be appropriately increased. The vertical angle is another crucial factor affecting the swirl. If the swirl height cannot reach near the spark plug, the vertical angle should be appropriately reduced. If there is too much dissipation due to the swirl radius reduction, the vertical angle should be increased appropriately. The orifice diameter affects the residual gas and jet penetration distance. If the jet penetration distance is insufficient, the orifice diameter should be reduced. If too much gas remains, the orifice diameter should be increased.

3.2. Influence of Nozzle Design on Jet Ignition

When the flame front propagates in the PC, the pressure increases rapidly, squeezing the unreacted/reacted gas through the nozzle as jet ejection. The jet ejection process can be divided into three stages, of which the dominant components are unburned gas, reaction intermediates, and reaction products, respectively. Hot high-speed jets with active radicals enhance the MC ignition through chemical, thermal, and turbulent effects. Numerous high-speed schlieren and chemiluminescence imaging studies have provided fundamental insights into jet ignition and concomitant quenching phenomena. Heat loss at the wall results in thermal quenching when the jet rushes through the nozzle. After entering the MC, the flow mixes with the unburned charge, and hydrodynamic quenching occurs. When the orifice diameter increases, the probability of the quenching phenomenon decreases, and the ignition mechanism gradually varies from turbulent jet ignition to flame ignition.

The lateral angle of the PC nozzle determines the scavenging efficiency, affecting the subsequent jet ignition process. However, the direct effect of the lateral angle on the jet orientation and penetration distance is relatively insignificant. Figure 7 shows the flame front propagation process for different lateral angle schemes. When the lateral angle is set to 10°, Case 1 presents the highest scavenging efficiency and the fastest flame propagation. However, because the swirl in the PC of Case 1 is not stable enough, the initial flame kernel develops asymmetrically. The flame does not spread evenly throughout the upper left side of the PC with the highest residual gas fraction. Although the asymmetric development of the initial flame kernel causes the jet to be uneven at 6°CA, as the combustion continues, the jet ignition becomes gradually uniform at 10°CA. Case 2, with a lateral angle of 0°, exhibited similar properties. The flame propagation of Case 2 is slightly lower than that of Case 1, but the jet symmetry is better due to the kinetic energy loss caused by the impact of the airflows.

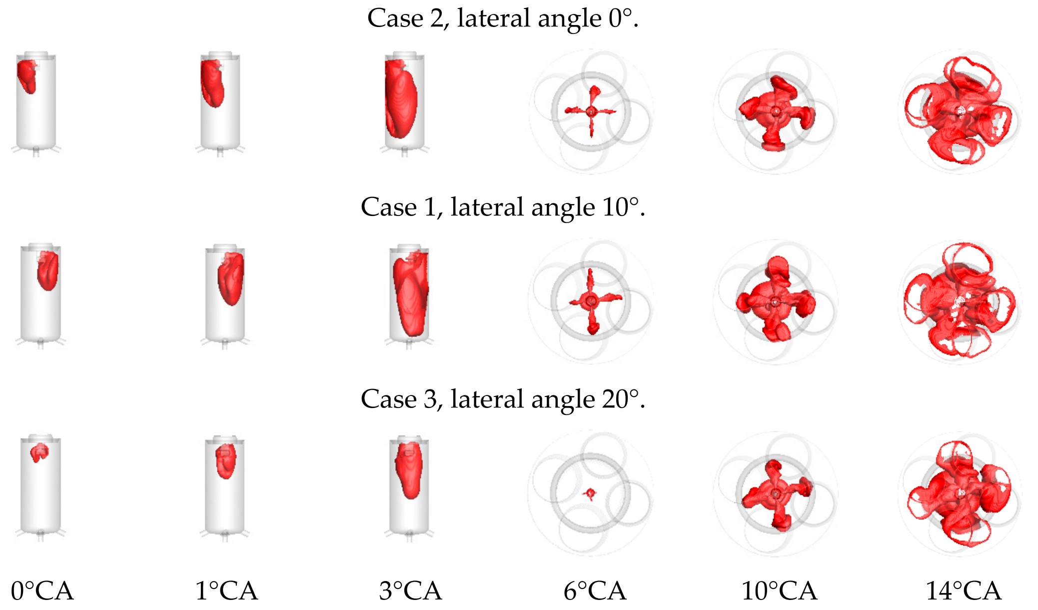

Figure 7. Flame propagation in the PC of Case 2, Case 1, and Case 3 during jet ignition.

In contrast, the swirl of Case 3, with a lateral angle of 20°, is stable, and the initial flame kernel develops symmetrically, as shown in Figure 7. However, since the area with the highest residual gas fraction coincides with the spark plug, the flame propagation speed is minimal. In a word, the previous scavenging effect dramatically influences the subsequent flame propagation speed. In addition, the importance of jet symmetry does not appear to be high. Even if a significant asymmetry occurs, it will gradually disappear during combustion.

Similarly to the lateral angle, the PC vertical angle can also affect jet ignition by determining the scavenging process. However, the vertical angle also has a more profound effect. The angle can affect the flow distribution in the squish and bowl areas by changing the jet orientation to control the flow separation at the piston throat. Figure 8 shows the flame front propagation process of different vertical angle schemes. The small-radius swirl in Case 4 and the low-height swirl in Case 5 reduce the scavenging efficiency and slow the flame propagation. When excluding the combustion phase difference in the three schemes, a direct comparison of Case 4 (12°CA), Case 1 (8°CA), and Case 5 (10°CA) shows that there are significant differences in the flow separation at the piston throat of each scheme. Case 4 has a minimum vertical angle of 120°, the jet orientation is biased toward the bottom of the piston, and the flame front fills the bowl area first. As the pressure in the bowl area increases, the jet deforms and is squeezed into the squish area. Case 5 has a maximum vertical angle of 140°, the jet orientation is biased towards the top of the piston, and the flame front first fills the squish area and then gradually develops towards the bowl area. Case 1 is a compromise between the first two schemes. The flame front reaches the bowl and squish areas almost simultaneously, finally filling the entire MC. Therefore, the PC with an optimized vertical angle has a short combustion duration and high stability.

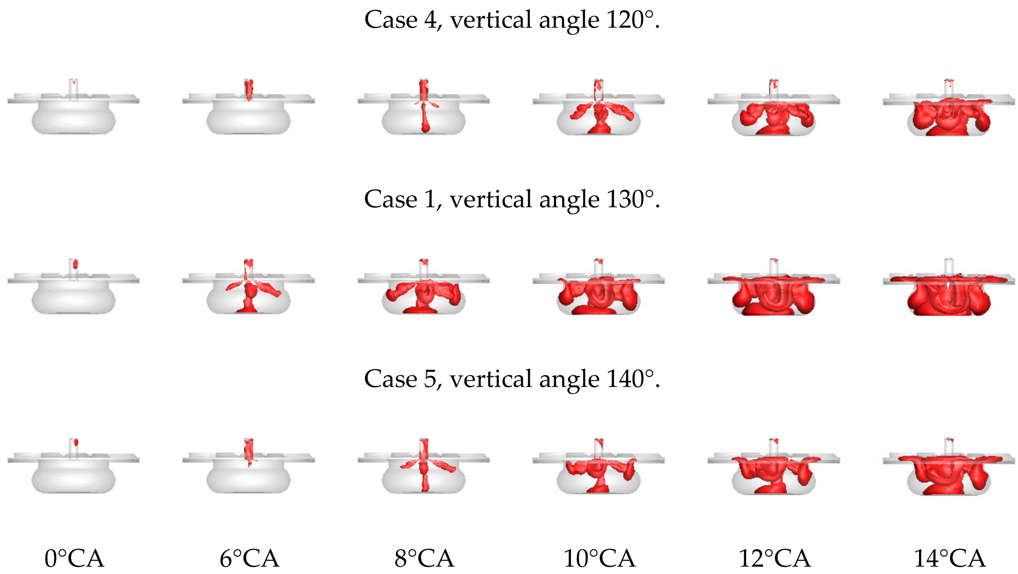

Figure 8. Flame propagation in the MC of Case 4, Case 1, and Case 5 during jet ignition.

The orifice diameter determines the scavenging efficiency and the jet velocity. In Figure 9, Case 6 has the lowest orifice diameter of 1.0 mm. The cross-sectional area of Case 6 is also the smallest, which significantly affects the scavenging efficiency. The ignition process is delayed, due to a large amount of residual gas in the PC. In the subsequent jet ignition process, driven by the considerable pressure difference, although the small orifice diameter increases the jet velocity, the benefits have approached the limit, which cannot offset the combustion phase delay that occurs at the initial stage of ignition. Case 7 has the largest orifice diameter of 1.6 mm. This case has the highest scavenging efficiency, but the unburned gas is more likely to escape as a cold jet, resulting in a decrease in the pressure and a short jet penetration distance. A short jet penetration distance increases the combustion duration and reduces flame uniformity. There is an optimal orifice diameter, considering the scavenging efficiency and the jet velocity, so that the combustion phase and jet penetration distance can meet the requirements. In the research of Antolini et al., the passive PC, with an orifice diameter of 1.2 mm, presents the fastest natural gas combustion speed, significantly higher than that of 1.0 mm and 1.5 mm, which is approximately consistent with the results of this paper.

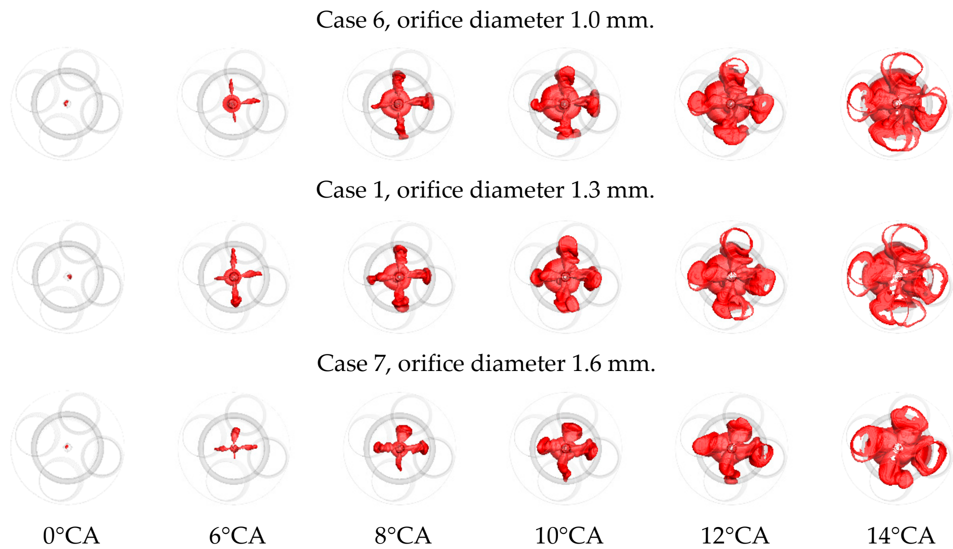

Figure 9. Flame propagation in the MC of Case 6, Case 1, and Case 7 during jet ignition.

Monitoring the heat release rate of the MC can confirm the jet ignition timing, which can be used as a boundary to distinguish between a cold jet and a hot jet, as shown in Figure 10. Among the factors, the flame speed and the orifice diameter present the most significant influence on the cold jet fraction. Case 1 has the best scavenging effect, and the flame speed in the PC is the fastest. More unburned gas near the nozzle is ignited before escaping, therefore, the cold jet fraction is the lowest. The effect of the orifice diameter is equally essential. Although the largest orifice diameter of 1.6 mm in Case 7 improves the scavenging and flame speed in the PC, the escape of unburned gas also increases. The results show that the cold jet fraction in Case 7, with the largest orifice diameter, is higher than that in Case 6, with the smallest orifice diameter, indicating that the performance loss caused by the unburned gas escape is greater than the enhancement of the flame speed. In addition to flame speed and orifice diameter, there are other interesting effects. Compared with the 0° lateral angle of Case 2, the 20° lateral angle of Case 3 presents a stable swirl and low flame speed in the PC. However, contrary to expectations, the cold jet fractions of Case 2 and Case 3 are comparable, suggesting that the inherent pressure gradient of the swirling flow played a role. A swirling flow is characterized by a low center pressure, as opposed to the characteristics of a high flame center pressure. The phenomenon retards the propagation of the pressure wave, which helps to restrain the cold jet and increases the jet ignition energy. The vertical angle of Case 5 is 140°, the flame speed in the PC is not high, and the mutual interference between the jets from the different orifices is minimal. These factors lead to an increase in unburned gas escape, similar to the effect of the large orifice diameter of Case 7.

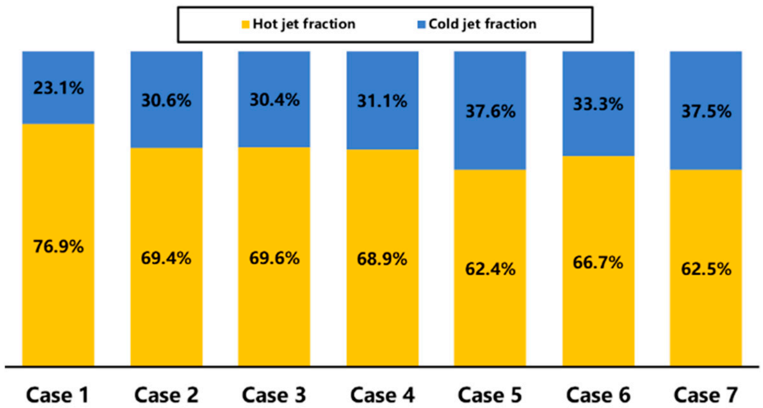

Figure 10. Mass fractions of cold and hot jets for 7 cases during jet ejection.

In summary, the nozzle design has a significant influence on jet ignition. The lateral angle affects the cold jet fraction. It should be increased if the cold jet produces insufficient jet ignition energy. In addition, the lateral angle also influences the jet symmetry, which is less critical because the flame homogenizes spontaneously as the combustion proceeds. Therefore, the lateral angle should be adjusted to balance the scavenging efficiency and the cold jet fraction, thereby improving the jet ignition energy. The vertical angle affects the jet orientation. If the jet flow separation at the piston throat is unbalanced, for example, if there is more flow in the bowl area than the squish area, the vertical angle should be increased, and vice versa. However, if the cold jet fraction rises, it may be caused by excessive vertical angles. The orifice diameter affects the jet penetration distance. The orifice diameter should be reduced if the jet penetration distance is insufficient. It is worth noting that, when there is a reduction in the orifice diameter, we must also consider the trade-off between scavenging and jet ejection.

3.3. Influence of Nozzle Design on the Main Combustion

After the combustion of the PC, hot jets eject and ignite the MC. Chemical, thermal, and turbulent effects enhance the flame in the MC. The three effects are derived from the improvement of the chemical reaction kinetics by active radicals, high temperature, and sufficient mixing of air and fuel. Compared with the single-point ignition of the traditional spark plug, turbulent jet ignition can significantly increase the ignition energy by about two orders of magnitude.

Figure 11 shows the MC and PC pressure and heat release rate curves of the cases during combustion. After ignition, the PC pressure increases, accompanied by cold and hot jets entering the main combustion chamber. Then, the pressure of the MC decreases slightly before burning, due to the downward movement of the piston. After jet ignition, the MC pressure rises rapidly and exceeds that of the PC. At this time, part of the gas mixture flows back into the PC. After the backflow finishes, the pressures of the MC and the PC are gradually balanced. The PC nozzle's lateral angle, vertical angle, and orifice diameter significantly impact the in-cylinder pressure, which is mainly reflected in the pressure peak and change rate. Figure 11a compares the in-cylinder pressure and heat release rate curves for lateral angles of 0°, 10°, and 20°. Appropriately increasing the lateral angle can improve the combustion phase and pressure peak. Still, as the angle increases and exceeds the critical value, the ignition energy decreases significantly, accompanied by an increase in the ignition delay. On the one hand, the center of the stable swirl is prone to retain the residual gas. On the other hand, the inherent pressure gradient of the swirling flow is opposite to the pressure wave generated by combustion, which is unfavorable for jet injection.

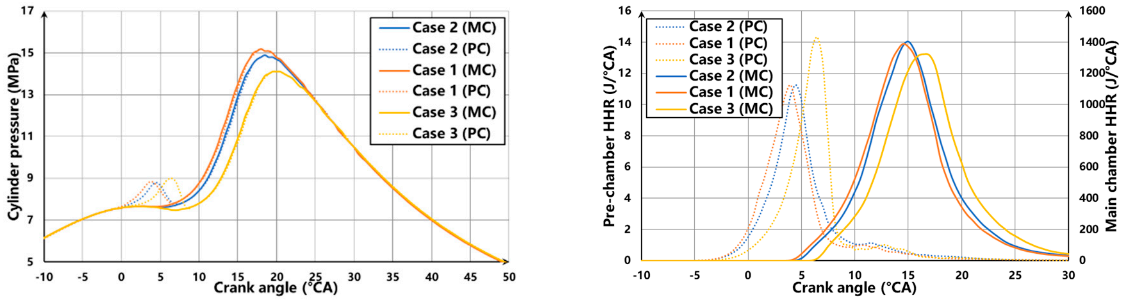

(**a**) Lateral angle (0°, 10°, and 20°)

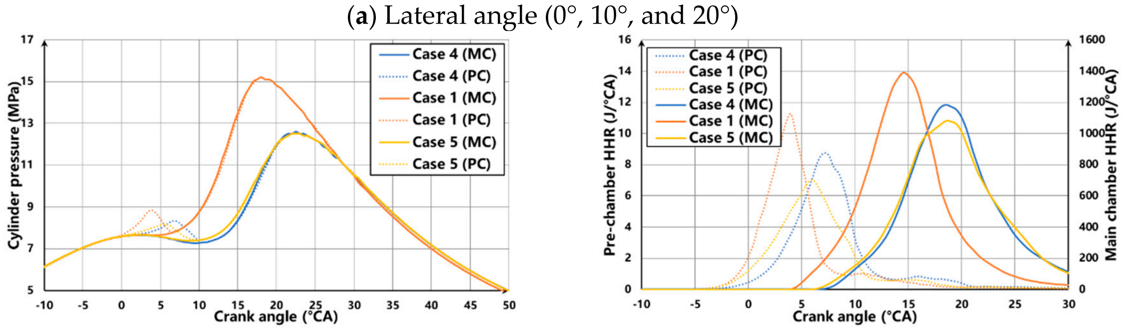

(**b**) Vertical angle (120°, 130°, and 140°)

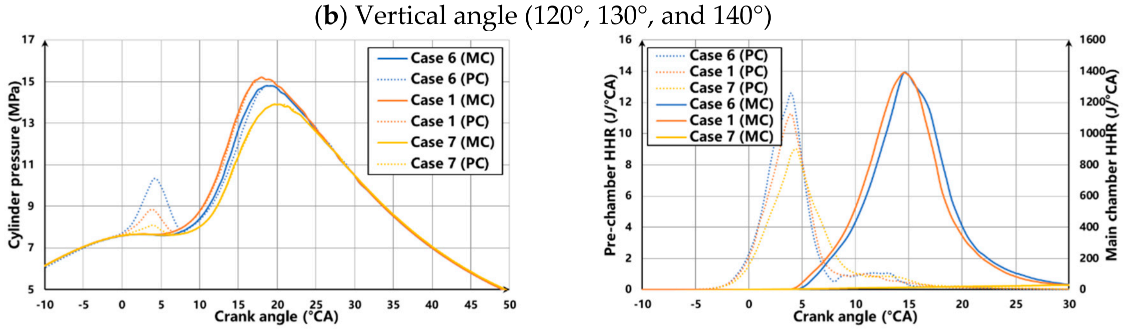

(**c**) Orifice diameter (1.0, 1.3, and 1.6 mm)

Figure 11. Cylinder pressure and heat release rate (HHR) of PC and MC for all cases during combustion.

Figure 11b compares the in-cylinder pressure and heat release rate curves with vertical angles of 120°, 130°, and 140°. It can be seen that the parameter sensitivity of the vertical angle is much higher than that of the lateral angle and orifice diameter. Increasing or decreasing the vertical angle from the optimal value will significantly decrease the ignition energy, but the mechanisms are different. The 120° small vertical angle design of Case 4 makes the jets of different nozzles interfere with each other, reduces the jet velocity, and then impacts the turbulence effect. The 140° large vertical angle design of Case 5 results in uneven flame distribution, with more jet flowing into the squish area. In addition, Case 5 presents a higher fraction of cold jets. Although the combustion phase is advanced, the ignition energy is decreased accordingly. Figure 11c compares the in-cylinder pressure and heat release rate curves for orifice diameters of 1.0 mm, 1.3 mm, and 1.6 mm. The scavenging effect of the PC with a large orifice diameter is the best, but the jet penetration distance and the ignition energy decline, resulting in reduced combustion efficiency.

After simulation ranking, four schemes are selected. The maximum pressure, knock frequency, EGR rate, and fuel consumption of the schemes and the original engine are tested on the bench, as shown in Figure 12. After the PC retrofit, the maximum pressure of the engine increases, while the knock remains near the original level. The EGR rate of Case 1 is significantly improved under operating Condition 2, i.e., under normal power. However, under the rated power of operating Condition 4, due to the high PC temperature affecting the scavenging charge, each scheme's EGR rate is challenging to increase compared to the original engine. It is worth noting that, under the joint influence of high PC temperature and small orifice diameter, the misfire phenomenon occurs in Case 6 under operating Condition 4. Finally, the PC retrofit presents significant economic advantages over the original engine. The fuel consumption rate can be saved up to 13.2% under normal power; however, the benefit relatively decreases under low load or rated power conditions.

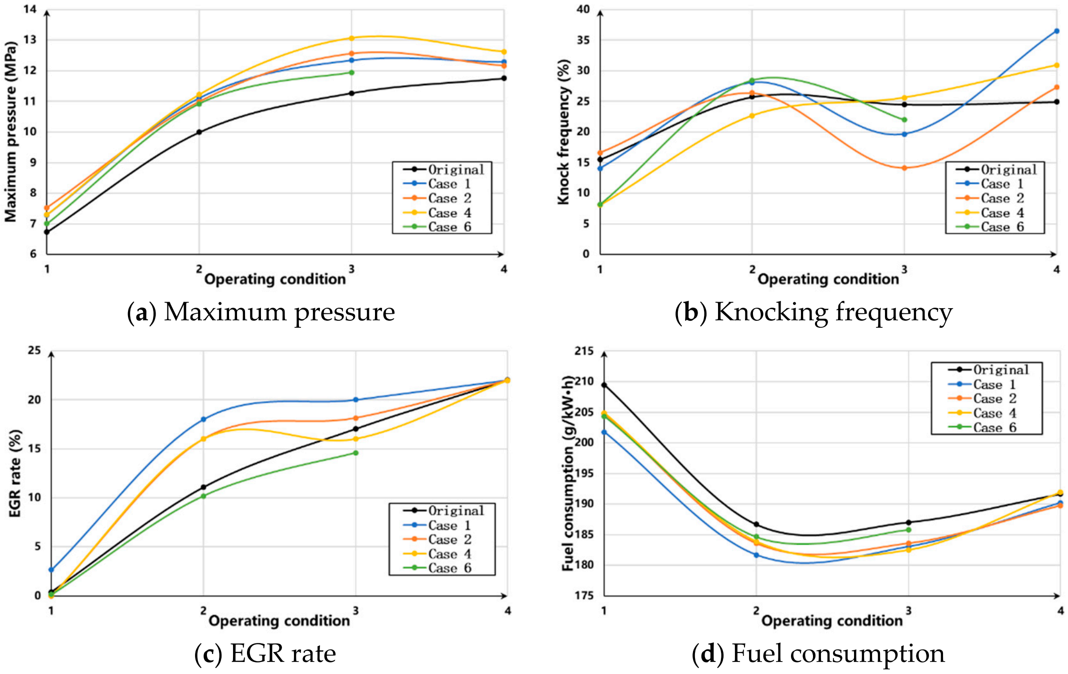

(**a**) Maximum pressure (**b**) Knocking frequency

(**c**) EGR rate (**d**) Fuel consumption

Figure 12. Experimental data of the selected schemes and original engine.

4. Conclusions

The plug-and-play passive pre-chamber (PC) is suitable for quick retrofit and improving fuel economy in realistic engines. In this paper, the influence of three key design parameters on ignition processes was numerically studied, including the lateral angle, the orifice diameter, and the vertical angle design. Seven PC schemes were numerically evaluated, and four were selected for the bench test. The characteristics of the scavenging process, turbulent jet ignition, and main-chamber combustion were investigated and analyzed.

Considering the trade-off of the ignition energy and scavenging efficiency, the ratio of the PC volume to the clearance volume is recommended to be 0.2~0.7%, and the area–volume of the PC is recommended to be 0.003~0.006 mm^{-1}. After the PC retrofit, the combustion duration can be shortened by 30~50%. The early combustion stage (mass fraction burned 10~50%) is significantly shortened, but the later combustion stage (mass fraction burned 50~90%) presents no noticeable improvement. Under normal power, the fuel consumption can be saved by 13.2%; however, the benefit is relatively reduced under low load or rated power conditions. In addition, the maximum pressure of the engine increases, while the knocking remains near the original level. The EGR rate is also improved, but the advantages of the PC become weakened at rated power due to the high temperature affecting the scavenging charge.

During the scavenging stage, the lateral angle determines the swirl intensity in the PC. The angle should be appropriately reduced if a stable swirl is formed in the PC. Otherwise, if the insufficient swirl intensity causes the airflows to collide, the lateral angle should be appropriately increased. The vertical angle is another crucial factor affecting scavenging. If the swirl height cannot reach near the spark plug, the vertical angle should be appropriately reduced. If the reduction in the swirl radius causes a significant dissipation, the vertical angle should be increased appropriately. The orifice diameter influences the jet penetration distance. The diameter adjustment should also consider the trade-off between scavenging and jet injection.

During the jet ignition stage, the lateral angle affects the cold jet fraction. The angle should be increased if the cold jet causes insufficient ignition energy. In addition, the lateral angle affects the jet symmetry, but the effect seems less critical. The vertical angle affects the jet's direction. If the jet separation at the piston throat is unbalanced, e.g., the flow in the bowl area is more significant than that in the squish area, the vertical angle should be increased, and vice versa. If the cold jet fraction rises, it may be due to an excessive vertical angle. Moreover, the vertical angle presents the most significant influence during the main chamber (MC) combustion stage. If the jet flames approach each other to interfere, the vertical angle should be increased. If the flame distribution appears to be out of balance, and the flame fraction in the squish area is too high, the vertical angle should be reduced.

Author Contributions: Writing—review and editing, W.L.; methodology and software, J.M.; validation and formal analysis, T.Z.; supervision, H.W.; project administration, J.P. All authors have read and agreed to the published version of the manuscript.

Funding: This research was funded by the National Key R&D Program of China (2022YFE0100100) and National Natural Science Foundation of China (52222604).

Institutional Review Board Statement: Not applicable.

Informed Consent Statement: Not applicable.

Data Availability Statement: Not applicable.

Conflicts of Interest: The authors declare no conflict of interest.

References

1. Joshi, A. *Year in Review: Progress towards Decarbonizing Transport and Near-Zero Emissions*; SAE Technical Paper 2023-01-0396; SAE International: Warrendale, PA, USA, 2023. [CrossRef]
2. Cardoso, J.; Silva, V.; Rocha, R.; Hall, M.; Daniela, E. Ammonia as an energy vector: Current and future prospects for low-carbon fuel applications in internal combustion engines. *J. Clean. Prod.* **2021**, *296*, 126562. [CrossRef]
3. Harindintwali, J.D.; Yuan, Z.; Wang, M.; Wang, F.; Li, S.; Yin, Z.; Huang, L.; Fu, Y.; Li, L.; Chang, S.X.; et al. Technologies and Perspectives for Achieving Carbon Neutrality. *Innov.* **2021**, *2*, 100180. [CrossRef]
4. Smith, I.; Chiu, J.; Bartley, G.; Jimenez, E.; Briggs, T.; Sharp, C. *Achieving Fast Catalyst Light-Off from a Heavy-Duty Stoichiometric Natural Gas Engine Capable of 0.02 g/bhp-hr NOX Emissions*; SAE International: Warrendale, PA, USA, 2018.
5. Hao, C.; He, J.; Zhong, X. Engine combustion and emission fuelled with natural gas: A review. *J. Energy Inst.* **2019**, *92*, 1123–1136.
6. Zhan, W.; Chen, H.; Du, J.; Wang, B.; Xie, F.; Li, Y. High Compression Ratio Active Pre-chamber Single-Cylinder Gasoline Engine with 50% Gross Indicated Thermal Efficiency. *ACS Omega* **2023**, *8*, 4756–4766. [CrossRef] [PubMed]

7. Payri, R.; Novella, R.; Barbery, I.; Bori-Fabra, O. Numerical and experimental evaluation of the passive pre-chamber concept for future CNG SI engines. *Appl. Therm. Eng.* **2023**, *230*, 120754. [CrossRef]
8. Frasci, E.; Cervone, D.; Nacci, G.; Sementa, P.; Arsie, I.; Jannelli, E.; Vaglieco, B.M. Comprehensive model for energetic analyses of a series hybrid-electric vehicle powered by a passive Turbulent Jet Ignition engine. *Energy Convers. Manag.* **2022**, *269*, 116092. [CrossRef]
9. Zhong, L.; Liu, P.; Zhou, L.; Wei, H. Experimental observation of turbulent jet ignition of pre-chamber with scavenging system for carbon dioxide diluted mixtures. *Proc. Combust. Inst.* **2023**, *39*, 4949–4958. [CrossRef]
10. Harrington, A.; Bassett, M.; Cooper, A.; Blaxill, H. *MAHLE Modular Hybrid Powertrain for Large Passenger Cars and Light Commercial Vehicles*; SAE International: Warrendale, PA, USA, 2022.
11. Riccardi, M.; De Bellis, V.; Sforza, L.; Tunestal, P.; Bozza, F.; Beatrice, C.; Lucchini, T. *Experimental and Numerical Analysis of an Active Pre-Chamber Engine Fuelled with Natural Gas*; SAE International: Warrendale, PA, USA, 2023.
12. Kraus, C.; Thamm, F.; Retzlaff, M.; Gadomski, B.; Fitz, P.; Härtl, M.; Hoppe, S.; Jaensch, M. *Highly Efficient and Clean Combustion Engine for Synthetic Fuels*; SAE International: Warrendale, PA, USA, 2023.
13. Harrington, A.; Hall, J.; Bassett, M.; Cooper, A. *Effect of Jet Ignition on Lean Methanol Combustion Using High Compression Ratio*; SAE International: Warrendale, PA, USA, 2023.
14. Zhou, L.; Ding, Y.; Li, A.Q.; Song, Y.; Liu, Z.; Wei, H. Experimental study of gasoline engine with EGR dilution based on reactivity controlled turbulent jet ignition (RCTJI). *Fuel* **2023**, *331*, 125744. [CrossRef]
15. Pielecha, I.; Szwajca, F. Combustion of Lean Methane/Propane Mixtures with an Active Prechamber Engine in Terms of Various Fuel Distribution. *Energies* **2023**, *16*, 3608. [CrossRef]
16. Zhao, Z.; Wang, Z.; Qi, Y.; Cai, K.; Li, F. Experimental study of combustion strategy for jet ignition on a natural gas engine. *Int. J. Engine Res.* **2022**, *23*, 104–119. [CrossRef]
17. Zhang, L.; Huang, Z.; Wang, T.; Zhao, N.; Cheng, H.; Chen, W. Lean combustion and emission performance of a gasoline direct injection engine with active pre-chamber. *Adv. Mech. Eng.* **2022**, *14*, 1–13. [CrossRef]
18. Chi, C.; Abdelsamie, A.; Thévenin, D. Transient Ignition of Premixed Methane/Air Mixtures by a Pre chamber Hot Jet: A DNS Study. *Flow Turbul. Combust.* **2022**, *108*, 775–795. [CrossRef]
19. Salerno, F.; Bargende, M.; Kulzer, A.; Grill, M.; Burkardt, P.; Günther, M.; Pischinger, S.; Villforth, J. *A Quasi-Dimensional Burn Rate Model for Pre-Chamber-Initiated Jet Ignition Combustion*; SAE International: Warrendale, PA, USA, 2023.
20. Liu, Z.; Zhou, L.; Wei, H. Experimental investigation on the performance of pure ammonia engine based on reactivity controlled turbulent jet ignition. *Fuel* **2023**, *335*, 127116. [CrossRef]
21. Chi, C.; Thévenin, D. DNS study on reactivity stratification with prechamber H2/air turbulent jet flame to enhance NH3/air combustion in gas engines. *Fuel* **2023**, *347*, 128387. [CrossRef]
22. Bucherer, S.; Rothe, P.; Sobek, F.; Gottwald, T.; Kraljevic, I.; Vacca, A.; Gal, T.; Chiodi, M.; Kulzer, A. *Experimental and Numerical Investigation of Spark Plug and Passive Pre-Chamber Ignition on a Single-Cylinder Engine with Hydrogen Port Fuel Injection for Lean Operations*; SAE International: Warrendale, PA, USA, 2023.
23. Zardoya, A.R.; Lucena, I.L.; Bengoetxea, I.O.; Orosa, J.A. Research on the new combustion chamber design to operate with low methane number fuels in an internal combustion engine with pre-chamber. *Energy* **2023**, *275*, 127458. [CrossRef]
24. Wu, X.; Feng, Y.; Gao, Y.; Xia, C.; Zhu, Y.; Shreka, M.; Ming, P. Numerical simulation of lean premixed combustion characteristics and emissions of natural gas-ammonia dual-fuel marine engine with the pre-chamber ignition system. *Fuel* **2023**, *343*, 127990. [CrossRef]
25. Zardoya, A.R.; Bengoetxea, I.O.; Martinez, A.L.; Lucena, I.L.; Orosa, J.A. Methodological Design Optimization of a Marine LNG Internal Combustion Gas Engine to Burn Alternative Fuels. *J. Mar. Sci. Eng.* **2023**, *11*, 1194. [CrossRef]
26. Liu, Z.; Wei, H.; Shu, G.; Zhou, L. Ammonia-hydrogen engine with reactivity-controlled turbulent jet ignition (RCTJI). *Fuel* **2023**, *348*, 128580. [CrossRef]
27. Liu, X.; Marquez, M.E.; Sanal, S.; Silva, M.; AlRamadan, A.S.; Cenker, E.; Sharma, P.; Magnotti, G.; Turner, J.W.; Im, H.G. Computational assessment of the effects of pre-chamber and piston geometries on the combustion characteristics of an optical pre-chamber engine. *Fuel* **2023**, *341*, 127659. [CrossRef]
28. Antolini, J.; Sementa, P.; Tornatore, C.; Catapano, F.; Vaglieco, B.M.; Desantes, J.M.; López, J.J. Effect of passive pre-chamber orifice diameter on the methane combustion process in an optically accessible SI engine. *Fuel* **2023**, *341*, 126990. [CrossRef]
29. Zhu, C.; Chakrapani, V.; Wooldridge, M. *An In-Cylinder Imaging Study of Pre-Chamber Spark-Plug Flame Development in a Single-Cylinder Direct-Injection Spark-Ignition Engine*; SAE International: Warrendale, PA, USA, 2023.
30. Frasci, E.; Rosa, R.N.; Moreno, B.P.; Arsie, I.; Jannelli, E. Impact of prechamber design and air–fuel ratio on combustion and fuel consumption in a SI engine equipped with a passive TJI. *Fuel* **2023**, *345*, 128265. [CrossRef]
31. Rajasegar, R.; Srna, A.; Novella, R.; Barbery, I. *Exploring the EGR Dilution Limits of a Pre-Chamber Ignited Heavy-Duty Natural Gas Engine Operated at Stoichiometric Conditions-An Optical Study*; SAE International: Warrendale, PA, USA, 2023.